

Biodistribution and Dosimetry of TRODAT-1: A Technetium-99m Tropane for Imaging Dopamine Transporters

P. David Mozley, James B. Stubbs, Karl Plössl, Stefan H. Dresel, Eleathea D. Barraclough, Abass Alavi, Luis I. Araujo and Hank F. Kung

University of Pennsylvania, Philadelphia, Pennsylvania, and Internal Dosimetry Systems of Oak Ridge, Oak Ridge, Tennessee

Technetium-99m TRODAT-1 is an analog of cocaine that selectively binds the presynaptic dopamine transporters. The primary purpose of this study was to measure its whole-body biokinetics and radiation dosimetry in healthy human volunteers. The study was conducted within a regulatory framework that required its pharmacological safety to be assessed simultaneously. **Methods:** The sample included 4 men and 6 women ranging in age from 22–54 yr. An average of 20 whole-body scans were acquired sequentially on a dual-head camera for up to 46 hr after the intravenous administration of 370 ± 16 MBq (10.0 ± 0.42 mCi) ^{99m}Tc TRODAT. The renal excretion fractions were measured from 12–24 discrete urine specimens. The fraction of the administered dose in 17 regions of interest and each urine specimen was quantified from the attenuation and background corrected geometric mean counts in conjugate views. Multiexponential functions were iteratively fit to each time-activity curve using a nonlinear, least squares regression algorithm. These curves were numerically integrated to yield source organ residence times. Gender-specific radiation doses were then estimated with the Medical Internal Radiation Dose technique for each subject individually before any results were averaged. **Results:** There were no pharmacological effects of the radiotracer on any of the subjects. The early planar images showed differentially increased activity in the nose, pudendum and stomach. SPECT images demonstrated that the radiopharmaceutical localized in the basal ganglia in a distribution that was consistent with selective transporter binding. Image analysis showed that the kidneys excreted between 20% and 32% of the injected dose during the first 22–28 hr postadministration, after which no more activity could be recovered in the urine. The dose limiting organ in both men and women was the liver, which received an average of 0.046 mGy/MBq (0.17 rads/mCi, range 0.14–0.22 rad/mCi). In the worst case, which was clearly an overestimation, it would have taken 22.7 mCi to deliver 5 rad to the liver. **Conclusion:** TRODAT may be a safe and effective radiotracer for imaging dopamine transporters in the brain and the body.

Key Words: technetium-99m; TRODAT-1; brain; computed tomography

J Nucl Med 1998; 39:2069–2076

In the brain, dopamine participates in the mediation of cognition, emotion and movement (1,2). It is involved in both the production and inhibition of several primary biological drives (3–5). In the gastrointestinal (GI) tract, dopamine helps to regulate motor tone and elaborate the gastrocolic reflexes.

The removal of free dopamine from the synaptic cleft is one of the primary mechanisms for regulating dopaminergic tone. The reuptake of free dopamine from the synaptic cleft is mediated by a macromolecular transporter embedded in the axonal membrane (6). Most drugs and diseases induce compensatory changes in transporter function before affecting the concentration of the postsynaptic dopaminergic receptors.

Drugs, such as cocaine (7) and some of its tropane derivatives, bind the transporter (8). As a result, these drugs block the reuptake of dopamine and exert a potent effect on both brain and bowel function (9).

Several radiolabeled tropanes have been successfully developed for imaging the central nervous system dopamine transporters in vivo (10–33). These agents have been remarkably effective in demonstrating normal (34) and abnormal (35–38) dopamine function in several disease states that have not been well demonstrated with other functional imaging techniques. Most of these radiopharmaceuticals have been labeled with positron emitting isotopes (39,40) or relatively expensive ^{123}I -based single photon emitters (41,42). Their success has led to efforts to produce cheaper, more widely available imaging agents for use in conventional medical settings (43–47).

Technetium-99m is the most commonly used radionuclide in diagnostic medicine (48). The 140 keV gamma ray it emits by isomeric transition to ^{99m}Tc has almost ideal physical imaging characteristics (49). Successfully labeling a transporter imaging agent with ^{99m}Tc would make it almost omni available at a small fraction of the cost required to produce most alternatives.

Technetium-99m, [2-[[[2-[[[3-(4-chlorophenyl)-8-methyl-8-azabicyclo[3.2.1]oct-2-yl]methyl](2-mercaptoethyl)amino]ethyl]amino] ethanethiolato(3-)-N₂,N₂' ,S₂,S₂']oxo-[1R-(exo-exo)]-, (TRODAT-1, Fig. 1) selectively binds the dopamine transporter (50). Using the rhenium-based complex as a surrogate, the inhibition constant, K_i , was found to be 14.1 nM (51). The striatal-to-cerebellar uptake ratios of TRODAT at 3 hr postintravenous injection have averaged 3.1:1 in anesthetized rats (51). Preclinical studies in nonhuman primates (52) and people (53) with SPECT have produced basal ganglia to occipital lobe contrast ratios of up to 3.5:1. Dynamic SPECT scans in baboons have demonstrated that indirect acting dopaminergic drugs decrease its uptake and increase its rate of elimination in the basal ganglia, whereas postsynaptic dopamine receptor antagonists do not (7). The findings have suggested that ^{99m}Tc TRODAT-1 may have several highly advantageous imaging characteristics for visualizing dopamine transporters.

Like any other radiopharmaceutical, the use of TRODAT in humans requires estimating its radiation dosimetry, that is, the amount of radiation energy deposited in each organ per unit dose of administered radioactivity (54). Image resolution generally improves with higher doses of radioactivity. Enhanced clinical efficacy usually follows as a direct result. Restraint is required, however, because higher doses may incur greater risks of radiation induced biological harm. Striking a balance between efficacy and safety requires measuring the dosimetry to each organ in the body. The process of estimating the radiation absorbed doses necessitates visualizing the whole-body at multiple time points after administration, including the neural

Received Jan. 13, 1998; accepted Apr. 13, 1998.

For correspondence or reprints contact: P. David Mozley, MD, 110-D Donner Building, H.U.P., 3400 Spruce St., Philadelphia, PA 19104.

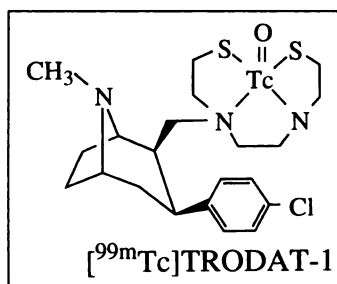


FIGURE 1. Chemical structure of ^{99m}Tc TRODAT-1.

networks of the bowel that sometimes receive less attention than brain studies.

MATERIALS AND METHODS

The design was similar to several others that we have already reported (55–58).

Accrual and Assessment of Subjects

The protocol was approved by the local Committee on Research Involving Humans and the U.S. Food and Drug Administration (IND# 56,623). Healthy volunteers were recruited through advertisements in local papers and by word of mouth from other volunteers. Structured medical histories were taken and physical examinations were performed before inclusion. None of the volunteers had a known history of a health problem that could have significantly affected the biodistribution or elimination of the radioligand at the time of study. None of the subjects were on any medications at the time of the study other than oral contraceptive pills. Only one urine drug screen turned up positive. A 54-yr-old accountant took diphenhydramine for allergies 48 hr before the procedure, and the laboratory detected it.

The final sample included 4 men and 6 women (mean age 33.7 ± 11.3 yr; age range 21–54 yr; 5 were Caucasian, 3 African American, 1 Hispanic and 1 Asian American). The 4 men had an average weight of 79.6 ± 7.2 kg (175 ± 16 lb) and a mean height of 173.6 ± 4.7 cm (68.4 ± 1.9 in.). The 6 women weighed an average of 65.6 ± 1.9 kg (148 ± 17 lb) and had a mean height of 167.5 ± 4.8 cm (65.6 ± 1.9 in.). The average education was 15.2 ± 2.4 yr (range 12–18 yr). All the subjects were employed except for 1 man who had a generally good vocational history but was temporarily between jobs.

Clinical Assessment Procedures

The baseline clinical laboratory tests included a complete blood cell count with differential, serum electrolytes, liver enzymes and thyroid function tests. Levels of creatinine, blood urea nitrogen, glucose, cholesterol, triglycerides, albumin and total protein were also assayed. Pregnancy was ruled out with measurements of β -human chorio-gonadotropic levels. Routine urinalyses and urine toxicology screens were performed after obtaining explicit consent for drug testing. The blood tests were repeated 1, 4 and 24 hr after the administration of the radiopharmaceutical. The urine tests were repeated once after 24 hr.

Electrocardiograms (EKGs) were performed. Continuous three-lead tracings began 15–30 min before administration of the radiopharmaceutical. They were continued for 60 min after administration and then once every 10 min for the next hour. Discrete 12-lead tracings were obtained intermittently. A cardiologist formally reviewed the tracings.

Vital signs were taken about once every 30 sec over the same time interval.

Radionuclide

Freshly eluted (no-carrier-added) ^{99m}Tc -pertechnetate (TcO_4^-) was obtained commercially from a ^{99}Mo generator (Mallinckrodt, Inc., St. Louis, MO).

Radiolabeling

The radiolabeling process began by dissolving 200 μg of dried free ligand, TRODAT-1, in 100 μl ethanolic HCl (100 μl HCl (2N) in 2 ml EtOH) and 200 μl of HCl (2N). To this solution, 50 μl of a sodium EDTA-solution (0.05 M) and 800 μl of a tin (Sn)-glucoheptonate solution was added (40 μg Sn(II)Cl₂ and 400 μg sodium glucoheptonate per ml solution) followed by 100–200 μl ^{99m}Tc -pertechnetate (TcO_4^-) in normal saline (in a range of 20–30 mCi) and 500 μl water. The vial was sterilized by autoclaving for 30 min at 16 atm and 121°C. After cooling to room temperature in an ice bath over 15 min, 800 μl of a fortified phosphate buffer (pH 6–7) were added.

The radiochemical purity (RCP) was determined by reversed-phase high-performance liquid chromatography analysis on a PRP-1 column (250 \times 4.1 mm) with an acetonitrile/DMGA buffer (pH 7) in a ratio of 80:20 and a flow rate of 1 ml/min. The retention time of ^{99m}Tc TRODAT-1 was about 11 min under these conditions. The results were corroborated with a partition method for estimating radiochemical purity. In a test tube, 1 ml of a saturated aqueous sodium bicarbonate (NaHCO_3) solution and 1 ml of an ethyl acetate/hexane (1:1; vol.) mixture was placed. Then 10 μl of the ^{99m}Tc TRODAT-1 solution was added and the mixture was vortexed for 60 sec. The test tube was capped and put upside down into a centrifuge. The tube was centrifuged and a sample was drawn through the cap with a clean syringe (aqueous layer). The test tube was turned over and a clean sample of organic layer was removed. A micropipette (1 λ) was filled with a sample of the aqueous layer and another one with a sample of the organic layer. The micro pipettes were put into different test tubes and the activity of each test tube was counted using the gamma counter. The test tube with the sample from the top (organic) layer contained the ^{99m}Tc TRODAT-1 and the test tube with the sample from the lower (aqueous) layer contained all radioimpurities.

The radiochemical purity was calculated using the following equation:

$$\%[^{99m}\text{Tc}] \text{ TRODAT-1} = \frac{A_t}{A_t + A_b} \times 100, \quad \text{Eq. 1}$$

where A_t = activity of the top (organic) layer and A_b = activity of the lower (aqueous) layer.

The RCP had to be over 90% to be acceptable for administration. Pyrogenicity tests were performed before administration. The unused portion of the final product was retained for sterility tests.

Measurements of Linear Attenuation

An uncollimated transmission source was prepared by dissolving about 1000 MBq ^{99m}Tc in a 1600 ml sheet flood made of Lucite. The rectangular dimensions of the sheet flood were about the same size as the collimators on a dual-head, whole-body camera (Prism 2000, Picker International, Cleveland, OH). The flood was taped flat on top of the posterior projection collimator, which was always 40 cm from the surface of the anterior projection collimator on the upper head.

Nonattenuated scans of the transmission source were performed in the whole-body mode by acquiring images on the upper camera while the sheet source moved with it in tandem on the lower head. The scans were acquired for 10 min each over an excursion of 188 cm, which corresponded to 102 sec/pixel.

The imaging table was then replaced at a height that was designed to place the midcoronal plane of an average adult in the center of the field between the two collimators. A whole-body transmission scan was then performed for 20 min (205 sec/pixel). The other acquisition parameters were identical to the ones that were used to acquire the nonattenuated transmission images of the flood and the subsequent emission scans.

Emission Images

Each study began on a Saturday morning. The radiopharmaceutical was injected rapidly as a bolus through an indwelling catheter in an antecubital vein while dynamic images of the thorax and abdomen were acquired for 2 sec per frame for 60 frames in a 256×256 matrix. A series of static images were then acquired for 30 sec a frame for 16 frames without moving the collimators. These images were used to localize activity in organs such as the spleen, which did not retain enough activity to be visualized on the later images. The first whole-body scan was started 10 min after injection. Each whole-body scan was acquired in a 256×1024 matrix for either 10 or 20 min over a total excursion length of 188 cm. The pixel size was always 2.18 mm square, which corresponded to scanning times of 102 or 205 sec per pixel. The early scans were acquired for 10 min each. The delayed images were acquired for 20 min. A mean of 20.1 ± 5.6 whole-body images were acquired.

SPECT

To validate that the radiopharmaceutical was a selective transporter antagonist, SPECT images of the brain were acquired in some subjects about 2.5 hr after injection on a triple-headed camera equipped with fanbeam collimators (Prism 3000, Picker International). The images were reconstructed with a counting rate-dependent restoration filter. The modulation transfer function was generated from the line spread function of the camera (59). Chang's method was used to correct the SPECT scans for attenuation with a uniform ellipse (60).

Renal Excretion Fractions

Subjects were asked to micturate as often as possible during the first day of the study and collect their own urine overnight. If the time interval between voiding was less than 2 hr and the volume of the voided specimen was less than 200 ml, the specimens were collected in 1200-ml containers. If the interval was more than 2 hr or the volume was more than 200 ml, a 5-liter container was used. The subjects produced an average of 17 ± 3 specimens over 28–43 hr (range 13–24). Whole-body images of the urine specimens were acquired with the same parameters that were used to scan the subjects by laying the samples out flat on the imaging table. Corrections for attenuation were limited to accounting for absorption and scatter through the imaging table the specimens were laid on. Attenuation by the urine itself was assumed to be negligible.

Image Analysis

The images were exported into a graphics workstation (Sun Microsystems, Mountain View, CA). The image analysis package (RIA, by Thew et al., University of Pennsylvania, Philadelphia, PA) automatically measured the total number of counts in each 256×1024 image. An operator drew regions of interest (ROIs) around 17 different organs or tissues, the whole-body and an off-body portion of the air and an off-body portion of the imaging table. The regions were drawn on whichever scan showed the organ most clearly after magnifying the images 2–16 times to facilitate tracing. Most organ boundaries were placed on the first whole-body scan, but the colon was always better visualized on the later images. It was feasible to place testicular ROIs on the initial images of the men ($n = 4$). ROIs for the breasts in women ($n = 6$) were placed with less confidence on the transmission scans because there was no selective uptake in this sample to show their true boundaries. The ROI for the nasal mucosa corresponded to a functional area of differentially increased uptake near the nose, which could be easily appreciated in most subjects. The thyroid could only be visualized in two volunteers. In the remainder of the sample, the ROI representing the thyroid was large and stylized to reflect the nonspecific activity in the region of the thyroid fossa. The kidneys could not be visualized well in the anterior projection,

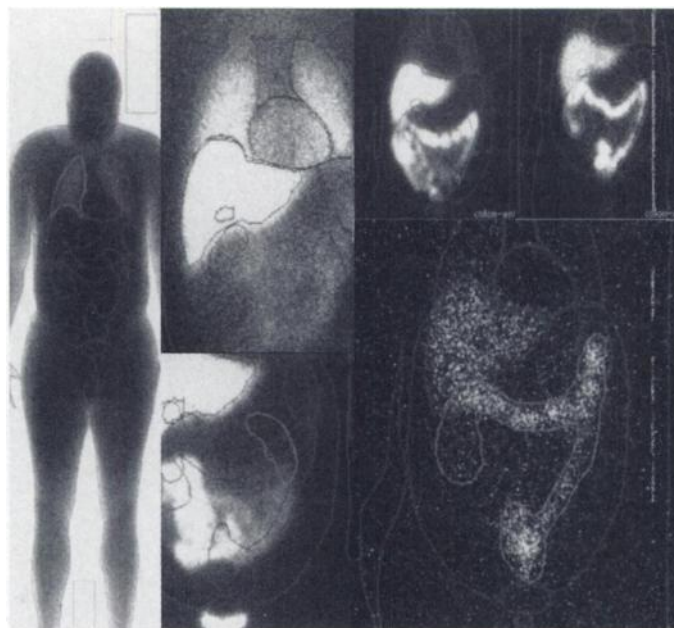


FIGURE 2. Representative transmission and emission images of 35-yr-old man.

so the regions for them were placed by flipping the posterior ROIs. Regardless of which scan the ROI originated from, it was cut and pasted into a single master set. Once the set was complete, the ROIs were transposed onto all the other images, including the transmission scans through air and the subject. It was occasionally necessary for an operator to move the entire set of ROIs as a single unit to correct for repositioning errors between scans. In a few cases, the position of the kidneys was not rigidly fixed and required compensation. It was also necessary to constantly adjust the size of the ROIs for viscus organs such as the urinary bladder and stomach to account for normal changes in volume. With the colon, each ROI had to be extensively revised throughout the study as it initially represented just the cecum and finally included the rectum. The last image that showed the colon best was used to estimate attenuation on the transmission scans. The ROI for the body almost always required minor revisions to correct for differences in pelvic tilt and the position of the feet. Otherwise, the individual ROIs were rarely manipulated independently of the other regions in the set. An automated subroutine measured the number of counts in these ROIs. A representative example is shown in Figure 2.

Calculating the Activity in an Organ

Background corrections were performed by subtracting the product of the mean counts per pixel in the off-body ROI and the number of pixels in the ROI for an organ from the total number of counts in the ROI for that organ. The impact of this maneuver on the initial images was trivial. The low counting statistics and the large decay correction factors (>150) associated with the delayed images led to a mean reduction of about 17% in the whole-body ROI at 42 hr.

Attenuation corrections were applied from the experimentally measured ratio of counts in the transmission scans of the subjects on the imaging table and the forward-decay corrected counts in the nonattenuated transmission scans through air.

Geometric means for each pair of decay, attenuation- and background-corrected conjugate ROIs were calculated by multiplying the net anterior counts by the net posterior counts and taking the square root of the product. The fraction of the injected dose at each time point was then estimated by dividing the corrected geometric mean number of counts in each ROI or urine specimen

TABLE 1
Residence Times for Technetium-99m TRODAT-1

Source organs	Mean (hr)	Minimum (hr)	Maximum (hr)	%s.d.*
Brain	0.11	0.08	0.13	15%
Breast	0.12	0.07	0.16	29%
Heart	0.19	0.14	0.31	29%
Kidneys	0.57	0.30	0.77	32%
Liver	3.24	2.42	3.81	11%
Lungs	0.70	0.48	1.21	31%
Spleen	0.20	0.07	0.38	46%
Thyroid	0.018	0.006	0.032	41%
Urinary bladder	0.34	0.25	0.50	20%
Remainder	1.17	0.73	2.09	39%
Whole body	7.65	7.33	8.04	3%
% Urine	25%	20.3%	31.5%	19%

*%s.d. = percent standard deviation (s.d./mean).

by the net geometric mean number of counts in the initial whole-body image.

Checks were performed by adding the fraction of the dose in the ROI representing the whole body to the fraction of the dose excreted in the urine up until that time, and comparing the sum to the total number of counts in the first set of emission images.

Organ Residence Times

Time-activity curves were generated directly from the experimental data for the brain, colon, gallbladder, heart, kidneys, liver, lungs, salivary glands, spleen, stomach, thyroid, urinary bladder and the whole abdominal compartment excluding the urinary bladder. Multiexponential functions were iteratively fit to each time-activity curve using a nonlinear least squares regression algorithm. These curves were numerically integrated to yield source organ residence times. Whole-body retention was estimated from the ROI encompassing the entire body.

The experimental measurements of activity voided in the urine were used to model the renal excretion rates. Parameters from the curve fits of the cumulative urinary excretion measurements were used as input data for the dynamic bladder model. However, the residence times for the urinary bladder, and thus the dosimetry estimates that followed, were based on a theoretical bladder voiding interval of 4.8 hr, or 5 times a day (61).

Activity that was not excreted in the urine was assumed to be eliminated in the feces. The colonic data were fit to the International Commission on Radiation Protection (ICRP) 30 GI tract model to determine the small and large bowel residence times (62). The standard mass of tissue in each region of the gut was taken from ICRP 23 (63). An adjustment to the GI and the remainder of the body residence times was performed to conserve activity, in the form of residence times. The initial remainder of the body residence times were calculated as the total body residence times minus the sum of the other source organ residence times (all organs of Table 1 except the GI tract and urinary bladder). For this correction, the GI organs were considered to be part of the remainder of the body. Hence, the individual GI residence times and remainder of the body residence times were normalized to the sum of the previously calculated GI and remainder residence times. As a result, the total residence times (summed overall organ in Table 1) were forced to be consistent with the total-body residence times.

The residence times were used to estimate the absorbed doses with the Medical Internal Radiation Dose (MIRD) technique (64) using the MIRDSE3.1 software package. For the calculations in men, the mass of the organs and their spatial relationships with the

other bodily tissues were based on the (American) Adult Reference Man (65,66). The model assumed that the average man weighed 70 kg, which was less than the actual value of 79.6 kg in this sample. The calculations for the women were based on the Adult Reference Woman (53), even though the women in this sample were significantly taller and heavier than the model. The consequence was to overestimate the radiation absorbed doses because both models assumed that the source organs were smaller and closer together than they actually were. The organ doses were calculated for each subject individually before the results were averaged.

RESULTS

There were no subjective effects of the radiotracer on any of the volunteers other than a mild and transient burning sensation at the site of injection. The problem was limited to the initial subjects and was probably related to the ethanol (200 μ l) that the radiotracer was dissolved in. Diluting the dose in 3 ml of normal saline and reducing the rate of administration rectified the problem in the later studies. No changes in vital signs could be attributed to a drug effect. Pulse quickened in one subject who experienced urinary frequency, but it returned to baseline shortly after micturation. There were no changes noted on physical examination. Over 1000 pages of continuous three-lead EKG tracings did not show any meaningful changes. Serially acquired 12-lead tracing occasionally produced computer readouts of "sinus bradycardia," "sinus arrhythmia," and in two subjects, "nonspecific T-wave abnormalities." However, two cardiologists independently concluded that there were no differences between the baseline EKGs and the postadministration tracings. Specifically, there were no signs of an ionotropic drug effect similar to that expected with pharmacological doses of cocaine. There were no meaningful changes in any of the clinical laboratory assays that were performed 1, 4 and 24 hr after the administration of the tracer. Only one subject had a baseline abnormality on the clinical laboratory studies. This 42-yr-old man had elevated liver function tests that did not change significantly during the course of the study. Another 28-yr-old woman had a mild microcytic anemia detected as her hemoglobin count varied slightly around the lower limit of normal, but there were no signs of a catecholamine-like effect on hematology.

SPECT images showed selective localization in the basal ganglia of the brain. Planar images demonstrated differentially increased activity in the nasal mucosa, stomach and testes (Fig. 3).

Image analysis demonstrated that the radioactivity associated with TRODAT was relatively slow to penetrate the adipose tissues, an effect that was particularly noticeable in the lower extremities. It was excreted primarily by the liver. Image analysis of the urine specimens produced experimentally measured renal excretion fractions of 20.3%–31.25% during the first 28 hr of study (mean \pm s.d.: 25.2% \pm 4.7%). Urine specimens obtained after 28 hr did not have any detectable activity in them. Most of the remaining dose could be detected in the GI tract.

Radioactivity was taken up by the liver rapidly. The fraction of the dose in the liver then increased continuously, but minimally, on the initial images. It did not peak for more than 10 hr, after which the curves were essentially flat. Over 30% of the injected dose was still in the liver at the end of the study.

Activity in the left upper quadrant corresponding to the stomach could usually be seen on the very first whole-body scans (Fig. 4). During the next several hours, this activity became progressively more obscure. It could not be visualized at all once activity was excreted into the small bowel, and then the colon. Activity could be seen entering the cecum in less than

TABLE 2

Dose Estimates for Technetium-99m TRODAT-1

	Mean (mGy/MBq)	Mean (rad/mCi)	Min. (rad/mCi)	Max. (rad/mCi)	s.d. (%)
Liver	0.047	0.173	0.143	0.220	15
Kidneys	0.035	0.131	0.081	0.178	26
ULI wall	0.028	0.104	0.074	0.124	15
Spleen	0.023	0.085	0.042	0.158	42
Urinary bladder wall	0.020	0.074	0.051	0.090	19
LLJ wall	0.018	0.067	0.049	0.078	14
Gallbladder wall	0.016	0.060	0.052	0.073	12
Small intestine	0.016	0.058	0.041	0.070	16
Heart wall	0.015	0.057	0.043	0.070	12
Lungs	0.015	0.055	0.045	0.073	15
Thyroid	0.012	0.046	0.019	0.070	37
Adrenals	0.010	0.037	0.032	0.044	12
Pancreas	0.010	0.037	0.030	0.045	14
Ovaries	0.008	0.029	0.021	0.034	17
Uterus	0.007	0.024	0.019	0.029	14
Stomach	0.006	0.023	0.018	0.027	16
Bone surfaces	0.005	0.019	0.016	0.023	14
Breasts	0.005	0.019	0.008	0.032	53
Total body	0.005	0.019	0.016	0.021	11
Red marrow	0.004	0.014	0.012	0.016	11
Muscle	0.003	0.012	0.010	0.014	13
Thymus	0.003	0.011	0.009	0.013	11
Brain*	0.002	0.008	0.005	0.010	19
Skin	0.001	0.005	0.004	0.007	16
Testes	0.001	0.004	0.004	0.005	11
EDE	0.015	0.055	0.045	0.065	13
Effective dose	0.012	0.046	0.039	0.053	10

*All radioactivity in the whole brain.

ULI = upper large intestine; LLJ = lower large intestine; EDE = effective dose equivalent.

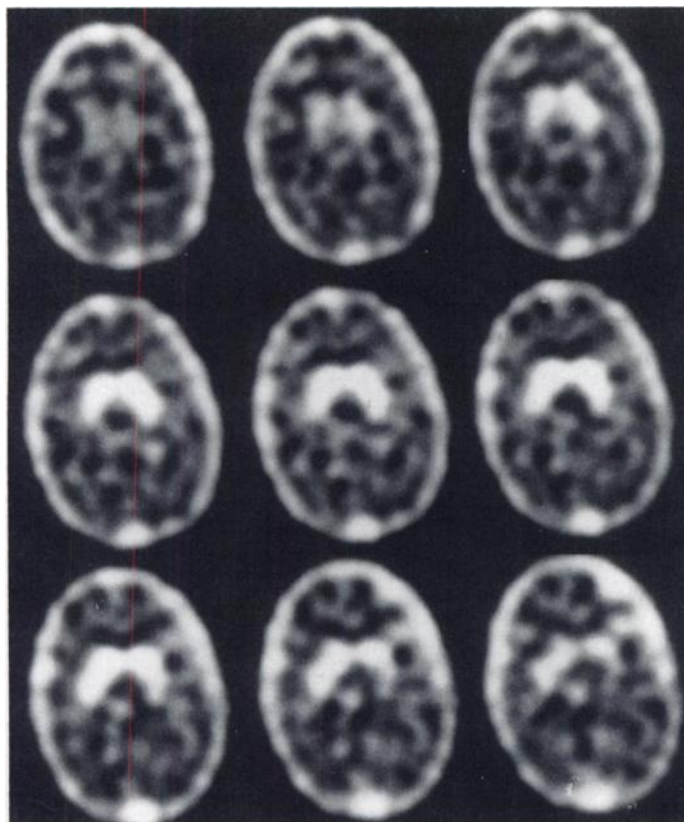


FIGURE 3. SPECT scan of the brain acquired 2.5–3 hr after administration.

6 hr. Despite the rapidity with which activity entered the lumen of the colon, the decay corrected fecal excretion fraction never exceeded more than 10% during the first 28 hr, or more than 35% during the first 43 hr.

Calculations of the residence times in each organ showed that the effective half-life of radioactivity associated with TRODAT was longest in the liver at 3.24 mCi-hr (range 2.42–3.81).

Table 2 lists the absorbed dose estimates for the entire sample. The differences between men and women were minimal when compared to the variability within each group. The dose limiting organ in both sexes was the liver, which received an estimated 0.046 mGy/MBq (0.17 rads/mCi). For female subjects, five organs were estimated to receive mean absorbed doses higher than 0.080 rad/mCi (liver: 0.19 rad/mCi; kidneys: 0.13 rad/mCi; upper large intestine: 0.11 rad/mCi; spleen: 0.095 rad/mCi; and bladder wall: 0.082 rad/mCi). The maximum organ absorbed dose for any female subject was 0.22 rad/mCi to the liver. The variability in organ absorbed doses was reasonable with only two organs showing percent s.d. above 30% (thyroid and spleen). These organs were not well visualized on the images, and were based on estimates from stylized ROIs. In

the case of the spleen, like that of the kidneys, it was not possible to keep the measurements from being confounded by the activity sweeping by in first the small bowel and then the splenic flexure of the colon. Substantially less variability was associated with the mean effective dose equivalent and effective dose, which were 0.059 and 0.049 rem/mCi, respectively.

For male subjects, five organs were estimated to receive mean absorbed doses higher than 0.060 rad/mCi (liver: 0.15 rad/mCi; kidneys: 0.13 rad/mCi; upper large intestine: 0.091 rad/mCi; spleen: 0.070 rad/mCi; and bladder wall: 0.063 rad/mCi). The maximum organ absorbed dose for any male subject was 0.16 rad/mCi to the liver. The variability in organ absorbed doses was reasonable with only one organ showing percent s.d. above 30% (thyroid). The mean effective dose equivalent and effective dose were 0.048 and 0.039 rem/mCi, respectively.

In nine subjects, the sum of the background and attenuation corrected geometric mean counts in the 256×1024 emission images plus the activity already voided in the urine never deviated by more than 5% from the total number of transmission corrected counts in the initial set of emission images. Most of the variation came at the later time points, particularly when the decay correction factors became large (>150 at 43 hr). At these time points, the counts in the ROI for the whole-body appeared to have slightly (2%) less activity in it than the ROI for the abdomen that it encompassed because only a very small fraction of the dose remained outside the abdomen and the pixel by pixel background subtraction applied to a larger number of pixels with no counts in them.

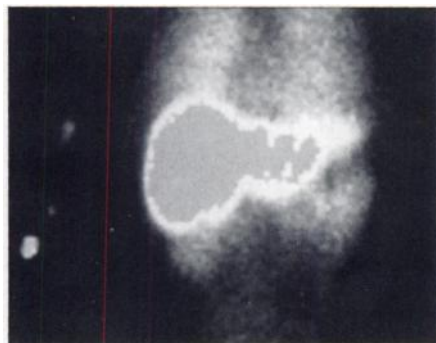


FIGURE 4. Early images demonstrating activity in the left upper quadrant corresponding to the stomach.

DISCUSSION

SPECT scans of the head and planar images of the body suggested that TRODAT selectively binds dopamine transporters. It is unlikely that the specific binding in either the brain or the stomach represents crossover serotonergic binding, as the affinity of the rhenium-surrogate for the serotonin transporters is weak at 360 nM in rat brain preparations. By contrast, the affinity for the dopamine transporter is 14 nM under the same conditions. The findings suggest ^{99m}Tc TRODAT may be an effective radiotracer for imaging transporters.

TRODAT appears to be pharmacologically safe in healthy volunteers. The lack of an effect from administering less than 50 ng (10^{-9} g) of radiolabeled TRODAT plus 0.2 mg of its unlabeled precursor is consistent with the observations that 50–200 mg of cocaine are required to produce a pharmacological response (67,68).

The radiation dosimetry of ^{99m}Tc TRODAT seems favorable. It could be argued that, rem for rem as currently calculated, the biological potential of the photon that is produced by the isomeric transition of ^{99m}Tc is less hazardous than the Auger electrons associated with radioiodinated pharmaceuticals. The selectivity of the parent compound for the dopamine transporters, its lack of a pharmacological effect and its favorable radiation dosimetry profile suggest that TRODAT may be yet another useful imaging agent for noninvasively visualizing dopamine transporters in the brain and the peripheral nervous system.

The lack of metabolism to free pertechnetate may make this tracer particularly useful for imaging transporters in the stomach. The accumulation of some ^{123}I -labeled transporter ligands in the stomach is much more intense, for example, but cannot be differentiated from free ^{123}I . This may be an important advantage, since the gastric distress that ensues as an untoward side effect of treatment with anti-Parkinsonian drugs is mediated by dopaminergic receptor activation. Dopamine may also play a role in the pathophysiology of irritable bowel syndrome, since the disorder can be palliated by selective dopaminergic antagonists that do not cross the blood-brain barrier.

Unlike cocaine and several of its tropane derivatives (69), TRODAT is excreted primarily by the hepatobiliary system. Some renal excretion occurred early, but could not be detected after about 28 hr. The maximum renal excretion fraction in this sample was only 32%. The actual percentage of the radioactivity excreted in the feces during the first 46 hr was small, averaging less than 1% of the injected dose and, theoretically, less than 35% of the decay-corrected dose. It follows that dose estimates based on imaging collections of excreted feces would have egregiously underestimated the colonic dosimetry. Relying exclusively on the images also obviated any potential problems with activity that could have recirculated through the enterohepatic system.

In contrast, transit through the bowel made it difficult to reliably measure activity in the kidneys and spleen on the images. These organs could barely be visualized on the initial flow images, and activity in the overlying colon frequently obscured them completely. For this reason, dose estimates to the kidneys were associated with a large degree of uncertainty. It was clear, however, that the values were overestimated because activity in the overlying bowel was always included in the ROIs for the kidneys. The dose estimates to the urinary bladder were based on a theoretical voiding interval of 4.8 hr, or 5 times a day. In clinical practice, the absorbed dose to the urinary bladder wall can probably be reduced substantially by encouraging subjects to micturate right after the neuroimaging procedure.

Even less confidence was associated with the estimated doses to the thyroid. The gland was only visualized in two subjects, and then only poorly. The lack of pertechnetate uptake by the thyroid, salivary glands and gastric mucosa is consistent with quality control procedures, which always showed that more than 90% of the injected dose was bound to the parent compound. It is also consistent with metabolite analyses in studies of nonhuman primates that showed TRODAT to be relatively stable *in vivo*.

The highest level of confidence could be placed in the sum of the activity in the whole body plus the activity excreted in the urine. In nine subjects, the background and attenuation corrected values rarely deviated from the total activity on the first emission image by more than 2%, and, except in one case, never varied by more than 5%. This is remarkable because the decay correction factors became large at the later time points (>150). Fractionating the urine into 12–24 specimens amounted to many quality control checks for showing that activity was conserved during each clinical measurement.

The small but definitely prolonged activity in the lungs is consistent with the observation of relatively prolonged plasma activity in nonhuman primates (52). This suggests that there could be several small compartments with relatively constant activity in them. Many organs could never be visualized on the images. Using physical decay only (PDO) after the last measurement (70) in these circumstances to model the time activity curves (TACs) tended to insure that the dose estimates remained conservative, since even small sequestrations of the initial dose can have a large impact on the area under the TACs (71). However, the size of the overestimates that follow are directly proportional to the physical half-life of the radiopharmaceutical, and indirectly proportional to the physiological rate of elimination in the large compartments, with faster rates leading to larger errors. The half-life of ^{99m}Tc is only about 6 hr, and the rate of elimination for the radioactivity associated with TRODAT after 24 hr is exceptionally slow. Since the last measurement occurred more than seven half lives after administration, the effect of the PDO assumption was probably negligible in this study.

In contrast to several radiopharmaceuticals, few differences could be detected between the biodistribution in men and women. This is consistent with the findings in rats, where there were no differences between males and females in eight major organ systems (51). The only sex differences in rats were found in the brain. Use of the Standard Adult Female Phantom led to an overestimation of the radiation absorbed doses in women because the volunteers in this study were significantly taller and heavier than the model. As a result, the model assumed that the concentration of activity in the source organs was higher than it actually was, and closer to each other than they actually were. In fact, the highest dose estimate to the liver, the dose limiting organ, was generated in the tallest woman in the sample. This observation suggests that using the most extreme case as the basis for limiting the dose in research volunteers who will not personally benefit from the study is quite conservative.

Despite these potentially conservative assumptions, the radiation dosimetry estimates for TRODAT appear favorable. Images of the basal ganglia containing reasonably good counting statistics could be produced with significantly less than the maximum dose of TRODAT recommended (72) or allowed (73) by current safety guidelines for research volunteers. If the dose of TRODAT were limited by the worst case in any organ from a single outlier, then 840 MBq (22.7 mCi) would still conform to current safety guidelines for research volunteers.

CONCLUSION

In general, the findings confirm that it is possible to measure the whole-body biodistribution of ^{99m}Tc -labeled tracers with greater precision and finer temporal sampling than commonly reported. Specifically, the results indicate that TRODAT may be a useful imaging agent for studying the presynaptic dopamine transporters in the brain and the bowel.

ACKNOWLEDGMENTS

This study was partially supported by National Institute on Drug Abuse grant DA09469, National Institutes of Health (NIH) grant NS-24538 and NIMH grant MH-43880. The clinical laboratory studies performed by the General Clinical Research Center at the University of Pennsylvania Medical Center were made possible by NIH grant MO1-RR00040. Consultation by Dr. Igor Laufer, Professor and Chief of GI Imaging and Dr. Robin Rothstein of Gastroenterology was greatly appreciated.

REFERENCES

- McHugh PR. The neuropsychiatry of basal ganglia disorders: a triadic syndrome and its explanation. *Neuropsychiatry Neuropsychol Behav Neurol* 1989;2:239–247.
- Alexander GE, Crutcher MD, DeLong MR. Basal ganglia-thalamocortical circuits: parallel substrates for motor, oculomotor, "prefrontal" and "limbic" function. In: Uylings HBM, Van Edin CG, De Bruin JPC, Corner MA, Feenstra MGP, eds. *Progress in brain research*, vol 85. New York: Elsevier Science Publishers; 1990:119–146.
- Smith GP, Schneider LH. Relationships between mesolimbic dopamine function and eating behavior. *Ann New York Acad Sci* 1988;537:254–261.
- Leibowitz SF, Rossakis C. Mapping study of brain dopamine- and epinephrine-sensitive sites which cause feeding suppression in the rat. Pharmacological characterization of perifornical hypothalamic dopamine receptors mediating feeding inhibition in the rat. *Brain Res* 1979a;172:101–113;1979b;172:115–130.
- Silverstone JT, Fincham J, Wells B, Kyriakides M. The effect of the dopamine receptor blocking drug pimozide on the stimulant and anorectic actions of dextroamphetamine in man. *Neuropharm* 1980;19:1235–1237.
- Cooper JR, Bloom FE, Roth RH. *The biological basis of neuropharmacology*, 6th ed. New York: Oxford University Press; 1991:292–294.
- Fowler JS, Volkow ND, Wolf AP, et al. Mapping cocaine binding sites in human and baboon brain in vivo. *Synapse* 1989;4:371–377.
- Carroll FI, Abram P, Lewin AH, Parham K, Boja JW, Kuhar MJ. Isopropyl and phenyl esters of 3b-(4-substituted phenyl)tropan-2b-carboxylic acids. Potent and selective compounds for the dopamine transporter. *J Med Chem* 1992;35:2497–2500.
- Johanson CE, Fischman, M. The pharmacology of cocaine related to its abuse. *Pharmacol Rev* 1989;41:3–52.
- Carroll FI, Scheffel U, Dannals RF, Boja JW, Kuhar MJ. Development of imaging agents for the dopamine transporter. *Med Res Rev* 1995b;15:419–444.
- Calligaro DO, Eldefrawi ME. High affinity stereospecific binding of ^3H cocaine in striatum and its relationship to the dopamine transporter. *Membrane Biochem* 1988;7:87–106.
- Fowler JS, Volkow ND, MacGregor RR, et al. Comparative PET studies of the kinetics and distribution of cocaine and cocacethylene in baboon brain. *Synapse* 1992;12:220–227.
- Abraham P, Pitner JB, Lewin AH, Boja JW, Kuhar MJ, Carroll FI. N-modified analogues of cocaine: synthesis and inhibition of binding to the cocaine receptor. *J Med Chem* 1992;35:141–144.
- Goodman MM, Kung M-P, Kabalka GW, Kung HF, Switzer R. Synthesis and characterization of radioiodinated N-(3-iodopropen-1-yl)-2b-carbomethoxy-3b-(4-chlorophenyl)tropanes: potential dopamine reuptake site imaging agents. *J Med Chem* 1994;37:1535–1542.
- Scheffel U, Dannals RF, Wong DF, Yokoi F, Carroll FI, Kuhar MJ. Dopamine transporter imaging with novel, selective cocaine analogs. *Neuroreport* 1992;3:969–972.
- Carroll FI, Lewin AH, Boja JW, Kuhar MJ. Cocaine receptor: biochemical characterization and structure-activity relationships of cocaine analogues at the dopamine transporter. *J Med Chem* 1992;35:969–981.
- Wang S, Gao Y, Laruelle M, et al. Enantioselectivity of cocaine recognition sites: binding of (1S)- and (1R)-2 beta-carbomethoxy-3 beta-(4-iodophenyl)tropane (beta-CIT) to monoamine transporters. *J Med Chem* 1993;36:1914–1917.
- Meltzer PC, Liang AY, Brownell AL, Elmaleh DR, Madras BK. Substituted 3-phenyltropane analogs of cocaine: synthesis, inhibition of binding at cocaine recognition sites, and positron emission tomography imaging. *J Med Chem* 1993;36:855–862.
- Madras B, Spealman R, Fahay M, Neumeyer J, Saha J, Milius R. Cocaine receptors labeled by ^3H -2b-carbomethoxy-3b-(4-fluorophenyl)tropane. *Mol Pharmacol* 1989;36:518–524.
- Boja J, Carroll F, Rahman M, Philip A, Lewin A, Kuhar M. New, potent cocaine analogs: ligand binding and transport studies in rat striatum. *Eur J Pharmacol* 1990;184:329–332.
- Ritz M, Boja J, Grigoriadis D, et al. Hydrogen-3-WIN 35,065-2: a ligand for cocaine receptors in striatum. *J Neurochem* 1990;55:1556–1562.
- Kozikowski AP, Roberti M, Xiang L, et al. Structure-activity relationship studies of cocaine: replacement of the C-2 ester group by vinyl argues against H-bonding and provides an esterase-resistant, high-affinity cocaine analogue. *J Med Chem* 1992;35:4764–4766.
- Staley JK, Basile M, Flynn DD, Mash DC. Visualizing dopamine and serotonin transporters in the human brain with the potent cocaine analogue [^{125}I]RTI-55: in vitro binding and autoradiographic characterization. *J Neurochem* 1994;62:549–546.
- Shaya EK, Scheffel U, Dannals RF, et al. In vivo imaging of dopamine reuptake sites in the primate brain using single photon emission computed tomography (SPECT) and iodine-123 labeled RTI-55. *Synapse* 1992;10:169–172.
- Neumeyer JL, Wang S, Milius RA, et al. Iodine-123-2b-carbomethoxy-3b-(4-iodophenyl)tropane: high-affinity SPECT radiotracer of monoamine reuptake sites in brain. *J Med Chem* 1991;34:3144–3146.
- Neumeyer JL, Wang S, Gao Y, et al. N-w-fluoroalkyl analogs of (1R)-2b-carbomethoxy-3b-(4-iodophenyl)tropane (b-CIT): radiotracers for positron emission tomography and single photon emission computed tomography imaging of dopamine transporters. *J Med Chem* 1994;37:1558–1561.
- Innis RB, Baldwin RM, Sybirskia E, et al. Single photon emission computed tomography imaging of monoamine reuptake sites in primate brain with ^{123}I CIT. *Eur J Pharmacol* 1991;200:369–370.
- Boja W, Patel A, Carroll FI, et al. Iodine-125-RTI-55: a potent ligand for dopamine transporters. *Eur J Pharmacol* 1991;194:133–134.
- Cline EJ, Scheffel U, Bola JW, et al. In vivo binding of ^{125}I -RTI-55 to dopamine transporter: pharmacology and regional distribution with autoradiography. *Synapse* 1992;12:37–46.
- Laruelle M, Baldwin RM, Malison RT, et al. SPECT imaging of dopamine and serotonin transporters with [^{123}I]B-CIT: pharmacological characterization of uptake in nonhuman primates. *Synapse* 1993;13:295–305.
- Aronson B, Enmon JL, Izenwasser S, et al. Synthesis and ligand binding of h6-(2b-carbomethoxy-3b-phenyltropane) transition metal complexes. *J Med Chem* 1996;39:1560–1563.
- Carroll FI, Mascarella SW, Kuzemko MA, et al. Synthesis, ligand binding, and QSAR (CoMFA and classical) study of 3b-(3'-substituted phenyl)-, 3b-(4'-substituted phenyl)-, and 3b-(3',4'-disubstituted phenyl)tropane-2b-carboxylic acid methyl esters. *J Med Chem* 1994;37:2865–2873.
- Neumeyer JL, Tamagnan G, Wang S, et al. N-substituted analogs of 2 beta-carbomethoxy-3 beta-(4'-iodophenyl)tropane (beta-CIT) with selective affinity to dopamine or serotonin transporters in rat forebrain. *J Med Chem* 1996;39:543–548.
- Volkow ND, Fowler JS, Wang GJ, et al. Decreased dopamine transporters with age in healthy human subjects. *Ann Neurol* 1994;36:237–239.
- Tatsch K, Schwarz J, Mozley PD, et al. Relationship between clinical features of Parkinson's disease and presynaptic dopamine transporter binding assessed with [^{123}I]IPT and single-photon emission tomography. *Eur J Nucl Med* 1997;24:415–421.
- Frost JJ, Rosier AJ, Reich SG, et al. Positron emission tomographic imaging of the dopamine transporter with ^{11}C -WIN 35,428 reveals marked declines in mild Parkinson's disease [see comments]. *Ann Neurol* 1993;34:423–431.
- Innis RB, Seibyl JP, Scanley BE, et al. Single photon emission computed tomographic imaging demonstrates loss of striatal dopamine transporters in Parkinson's disease. *Proc Natl Acad Sci USA* 1993;90:11965–11969.
- Innis RB. Single photon emission tomography imaging of dopamine terminal innervation: a potential clinical tool in Parkinson's disease [Editorial]. *Eur J Nucl Med* 1994;21:1–5.
- Volkow ND, Ding YS, Fowler JS, et al. A new PET ligand for the dopamine transporter: studies in the human brain. *J Nucl Med* 1995;36:2162–2168.
- Wong DF, Yung B, Dannals RF, et al. In vivo imaging of baboon and human dopamine transporters by positron emission tomography using ^{11}C -WIN35,428. *Synapse* 1993;15:130–142.
- Yu D-W, Gatley SJ, Wolf AP, et al. Synthesis of carbon-11-labeled iodinated cocaine derivatives and their distribution in baboon brain measured using positron emission tomography. *J Med Chem* 1992;35:2178–2183.
- Kuikka JT, Akerman K, Bergstrom KA, et al. Iodine-123-labeled N-(2-fluoroethyl)-2b-carbomethoxy-3b-(4-iodophenyl)tropane for dopamine transporter imaging in the living human brain. *Eur J Nucl Med* 1995;22:682–686.
- Meegalla SK, Plossl K, Kung M-P, et al. Technetium-99m labeled tropanes as dopamine transporter imaging agents. *Bioconj Chem* 1996;7:421–429.
- Meltzer PC, Blundell P, Jones AG, et al. A technetium-99m SPECT imaging agent which targets the dopamine transporter in primate brain. *J Med Chem* 1997;40:1835–1844.
- Madras BK, Jones AG, Mahmood A, et al. Technetium-99m: a high affinity technetium-99m probe to label the dopamine transporter in brain by SPECT imaging. *Synapse* 1996;22:239–246.
- Tamagnan G, Gao YG, Baldwin RM, Zoghbi SS, Neumeyer JL. Synthesis of beta-CIT-BAT, a potential ^{99m}Tc imaging ligand for dopamine transporter. *Tetrahedron Lett* 1996;37:4353–4356.
- Zoghbi SS, Tamagnan G, Baldwin RM, et al. Synthesis of a dopamine transporter binding cyclopentadiene phenyltropane conjugate complexed with rhenium and ^{99m}Tc [Abstract]. *J Nucl Med* 1997;38:100P.
- Steigman J, Eckelman WC. *The chemistry of technetium in medicine*. Washington, DC: National Academy; 1992.
- Sorenson JA, Phelps ME. *Physics in nuclear medicine*, 2nd ed. Philadelphia: WB Saunders Co.; 1987.
- Meegalla SK, Plössl K, Kung M-P, et al. Synthesis and characterization of ^{99m}Tc -labeled tropanes as dopamine transporter imaging agents. *J Med Chem* 1997;40:9–17.
- Kung M-P, Stevenson DA, Plössl K, et al. Technetium-99m TRODAT-1: a novel technetium-99m complex as a dopamine transporter imaging agent. *Eur J Nucl Med* 1997;24:372–380.
- Kushner SA, McElgin WT, Kung M-P, et al. Kinetic modeling of ^{99m}Tc TRODAT-1: a novel compound for imaging the dopamine transporter. *J Nucl Med* 1999; in press.
- Kung HF, Kim H-J, Kung M-P, Meegalla SK, Plössl K, Lee H-K. Imaging of dopamine transporters in humans with technetium-99m TRODAT-1. *Eur J Nucl Med* 1996;23:1527–1530.

54. Sorenson JA, Phelps ME. Internal radiation dosimetry. In: *Physics in nuclear medicine*, 2nd ed. Philadelphia: WB Saunders Co.; 1987:197-218.
55. Mozley PD, Zhu XW, Kung HF, et al. The dosimetry of 3-Iodo-Schering 23390: quantification of the radiation burden to healthy humans. *J Nucl Med* 1993;34:208-213.
56. Mozley PD, Stubbs JS, Kung HF, et al. Biodistribution and dosimetry of ¹²³I IBF: a potent radioligand for imaging the D2 dopamine receptor. *J Nucl Med* 1993;34:1910-1917.
57. Mozley PD, Stubbs JB, Kim H-J, et al. Dosimetry of a D2/D3 dopamine receptor antagonist that can be used with PET or SPECT. *J Nucl Med* 1995;35:1322-1331.
58. Mozley PD, Stubbs JB, Kim H-J, et al. Dosimetry of an iodine-123-labeled tropane to image dopamine transporters. *J Nucl Med* 1996;37:151-159.
59. Kim H-J, Karp JS, Kung HF, Mozley PD. Quantitative effects of a count rate dependent Wiener filter on image quality: a basal ganglia phantom study simulating ¹²³I dynamic SPECT imaging [Abstract]. *J Nucl Med* 1993;34:190P.
60. Chang LT. A method for attenuation correction in radionuclide computed tomography. *IEEE Trans Nucl Sci* 1978;NS-25:638-643.
61. Cloutier RJ, Smith SA, Watson EE, Snyder WS, Warner GG. Dose to the fetus from radionuclides in the bladder. *Health Physics* 1973;25:147-161.
62. International Commission on Radiation Protection. ICRP publication 30. *Limits for intake of radionuclides by workers*. New York: Pergamon Press; 1979.
63. International Commission on Radiation Protection. ICRP publication 23. *Report of the task group on reference man*. Oxford: Pergamon Press; 1979.
64. Loevinger R, Berman M. MIRD pamphlet no. 1, revised. *A revised schema for calculating the absorbed dose from biologically distributed radionuclides*. New York: Society of Nuclear Medicine; 1975.
65. Cristy M, Eckerman K. Specific absorbed fractions of energy at various ages from internal photon sources. ORNL/TM-8381. Oak Ridge, TN: Oak Ridge National Laboratory Press; 1987.
66. Snyder WS, Ford MR, Warner GG, Watson SB. MIRD pamphlet no. 11. "S" *absorbed dose per unit cumulated activity for selected radionuclides and organs*. New York: Society of Nuclear Medicine; 1975.
67. Lange RA, Cigarroa RG, Yancey CW Jr, et al. Cocaine-induced coronary-artery vasoconstriction. *New Engl J Med* 1989;321:1157-62.
68. Moliterno DJ, Willard JE, Lange RA, et al. Coronary-artery vasoconstriction induced by cocaine, cigarette smoking, or both. *N Eng J Med* 1994;330:454-459.
69. Mozley PD, Stubbs JB, Kim H-J, McElgin W, Kung HF. Biodistribution and dosimetry of ¹²³I-labeled IPT. *J Nucl Med* 1996;37:151-160.
70. Gatley S. Estimation of upper limits on human radiation absorbed doses from carbon-11-labeled compounds. *J Nucl Med* 1993;34:2208-2210.
71. Selikson MH, Jaggi J, Mozley PD, et al. A proposal for minimum detectable compartment in MIRD dosimetry modeling. *Phys Med Biol* 1997;42:1605-1617.
72. National Council of Radiation Protection and Measurements. NCRP report no. 39. *Basic radiation protection criteria*. Washington, DC: National Council of Radiation Protection and Measurements; 1971.
73. Food and Drug Administration, HHS. *Radioactive drugs for certain research uses. Code of Federal Regulations 21, ch. 1 (4-1-89 ed.) part 361.1, paragraph (b) (3) (i)*. Washington, DC: Food and Drug Administration; 1989:206.